Journal of Hazardous Materials 181 (2010) 305–314

Contents lists available at ScienceDirect

Journal of Hazardous Materials

journal homepage: www.elsevier.com/locate/jhazmat

Combustion characteristics of particles of hazardous solid waste mixtures in a fixed bed

Ling Tao[a,*], Guangbo Zhao[a], Rui Sun[a], Qiang Wang[b]

[a] School of Energy Science and Engineering, Harbin Institute of Technology, 92 West Dazhi Street, Harbin 150001, Heilongjiang, PR China
[b] Liaoning Hongyanhe Nuclear Power Co. Ltd, Wafangdian 116319, PR China

ARTICLE INFO

Article history:
Received 9 December 2009
Received in revised form 19 April 2010
Accepted 5 May 2010
Available online 11 May 2010

Keywords:
Hazardous waste
Combustion characteristics
Fixed bed

ABSTRACT

Hazardous waste disposal is vitally important as industrial production increases. Grate furnaces are a common means to incinerate hazardous waste. In this present work, a fixed bed assembly is used to experimentally model combustion within grate furnaces. Combustion characteristics are examined and the effects of primary air rate, moisture, bed height and particle size on burning rate, ignition-front speed and temperatures in the bed are also investigated. The results indicate that a rising temperature front descends through the bed while weight loss remains constant during the main combustion stage. Primary air rates and moisture content are shown to have significant effects on burning rates and average ignition-front speeds. Bed height has no effect on burning rates but does have an effect on average ignition-front speeds. Particle size is found to have slight effects on burning rates while having no effect on average ignition-front speeds.

1. Introduction

Hazardous waste from industrial production is becoming an ever-increasing concern as economic development progresses. An estimated 10 million tons of hazardous waste is produced annually in China [1–4]. Moreover, a wide variety of industrial hazardous wastes is being created, most of which is harmful and very slow to decompose by natural processes. Such wastes cause enormous concern for human life and potentially huge damage to the environment. Under these circumstances, the development of adequate waste treatment processes is urgently needed.

In most countries, resource utilization, minimization and harmless treatment are the most important and widely used methods employed in disposing of hazardous waste. Currently in China, harmless treatment is the more suitable method. Incineration is widely used for its ability to reduce and decontaminate solid waste and maintain low levels of secondary pollution. Incineration has another advantage in that combustion of the organic component in wastes release energy that can be collected and exploited in waste heat boilers. Indeed, some solid wastes have the same heating value as coals.

Currently in use are several types of incinerators including rotary kilns, fluidized beds and grate furnaces. Of these three incinerators, grate furnaces have the least flexibility. However, grate furnaces cost less and have greater adaptability concerning particle size and higher heat efficiencies. Thus, they are usually the incinerators of choice when used in medium and small-scale waste disposal plants.

For this reason, the combustion characteristics and gas releases of the grate furnace should be studied to optimize combustion and reduce pollution. Hazardous wastes, as the raw material of the furnace, display a wide spectrum of physical and chemical characteristics. Fuel properties and incineration conditions, such as fuel type, particle size, fuel moisture and primary air rate, impact in a very complicated way on the combustion characteristics by changing heat generation, heat transfer and reaction rates. The combustion characteristics of municipal solid wastes, biomass and medical wastes have already been studied [5–13]. However, less studied have been the combustion characteristics of industrial hazardous wastes. In the present work, we address this aspect by discussing experiments of wastes particles in a fixed bed assembly.

2. Experimental

2.1. Combustion in a grate furnace: description and modeling

The various stages of waste combustion in a grate furnace are schematically depicted in Fig. 1. Solid waste is transferred into the furnace by a feeder and a uniform bed is formed. Waste is then transported forward by the grate. The combustion stages can be roughly identified according to temperature with four sequential zones in the furnace: namely (1) preheating and drying zone, (2)

* Corresponding author. Tel.: +86 451 86412908x534; fax: +86 451 86412528.
E-mail address: taolingsd@yahoo.com.cn (L. Tao).

0304-3894/$ – see front matter © 2010 Elsevier B.V. All rights reserved.
doi:10.1016/j.jhazmat.2010.05.012

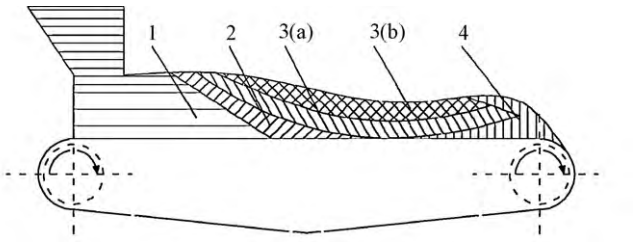

Fig. 1. Combustion zones in a grate furnace.

volatile devolatilization and combustion zone, (3) char combustion zone, and (4) ash residue burning-out zone. The waste bed is irradiated by the flame above the bed and the hot front arch immediately in the preheating and drying zone, which dries waste on the top surface of the bed. Next, the dried waste releases volatile substances that start to burn above the bed surface. The resulting combustion flame radiates the waste bed, thus constituting the volatile devolatilization and combustion zone. After the release and burning of volatiles, char in the waste bed also starts burning at a temperature constituting the highest in the waste bed. The char combustion zone can itself be divided into two subzones. When air is supplied from below, the char in the bottom reacts in an oxygen-rich atmosphere that creates a waste layer of oxidized char. Char on top of the bed reacts in an oxygen-poor atmosphere as flue gas from char oxidation at the bottom passes to the top. This leads to a reducing reaction of combustion gas with char, thus creating a layer of reduced char. At the end of the process, some char remains burning in the burn-out zone associated with ash residue.

From a time-lapse perspective, we consider a vertical cross-section of the waste bed during the combustion process as it is transported on the grate. With a constant grate speed, the horizontal position on the grate identifies the combustion stage of waste in this continuous process. While waste moves horizontally, air and combustion gases travel upwards from the bed. As the reaction progresses, an evaporation and combustion layer is initiated at the top surface of the bed and then descends through the bed. Waste in this cross-section experiences an evolving sequence of processes comprising heating-up, moisture evaporation, pyrolysis, gas combustion, and char combustion. Although air and combustion gases pass through the waste bed in a matter of only a few seconds, the waste bed moves very slowly usually spending 1 hour or even longer on the grate. Hence, temperature gradients and concentration gradients of chemical species in the direction of motion of the bed are negligible compared with those in the direction of gas flow, indicating that heat and mass transfer can be ignored in the direction of waste transport. Based on the above description, continuous and steady combustion of the waste bed on the grate can be simulated by an evolving one-dimensional model, as outlined in Fig. 2. The model assumes a layer of waste particles that have similar geometrical shape, as well as physical and chemical characteristics. Primary air flows upwards from the bottom. The volatiles, the combustion gas and the flue gas flow in the same direction with the primary air. Combustion characteristics in this flow direction are the emphasis in our work.

2.2. Fixed bed description

Fig. 3 shows a schematic diagram of the experimental facility. The facility consists of a cylindrical combustion chamber, gas burner and gas supply system, grate, air supply system, temperature measuring system, combustion gas sampling and measuring system, and weight measuring system. The height of the cylindrical chamber is 1500 mm with an inner diameter of 180 mm. The chamber consists of 50 mm thick high-alumina refractory, which is able to withstand temperatures up to 1300 °C, 5 mm thick protective casing of 1Cr18Ni9Ti steel and 150 mm thick insulation made of aluminum silicate refractory fiber from the inner to the outer layer. A grate of diameter 178 mm is located at the bottom of the chamber. Made from stainless steel, it has 96 holes of 7 mm diameter, representing an open area of 14.8%. The primary air is fed into the chamber from the bottom through the grate without preheating. Ten thermocouples are arranged along the central axis of the chamber, the positions of which are presented in Table 1. Thermocouples 1–9 are placed above the grate to measure the temperature of the flue gas (t1), the temperature of the propane flame (t2), the temperature of combustion gas over the bed (t3) and the bed temperature (t4–9), while thermocouple 10 is placed under the grate to measure the temperature of the primary air. A weighing gauge suspends the whole chamber to monitor the weight loss during the experiment. A combustion gas sampling port is arranged on the sidewall at a distance of 388 mm above the grate. It is used to con-

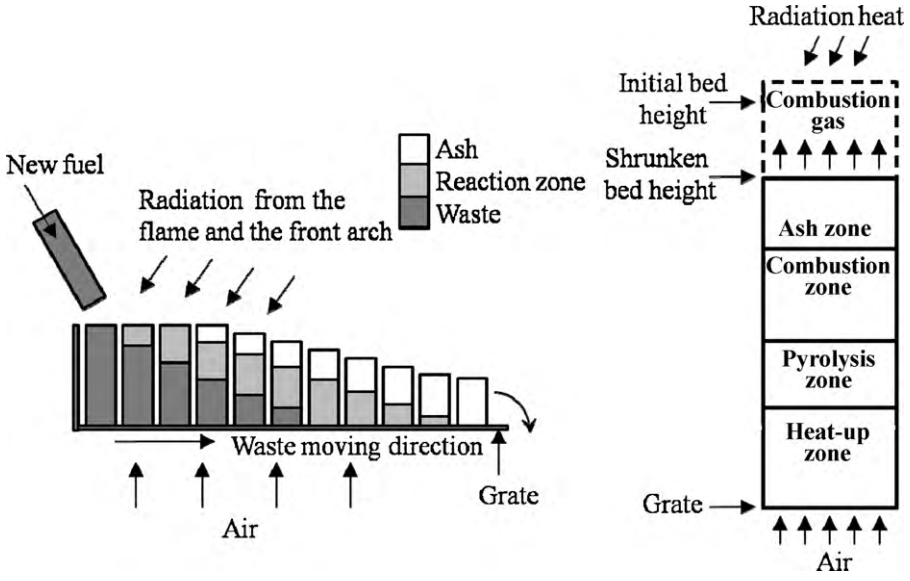

Fig. 2. Model process of waste combustion in a grate furnace.

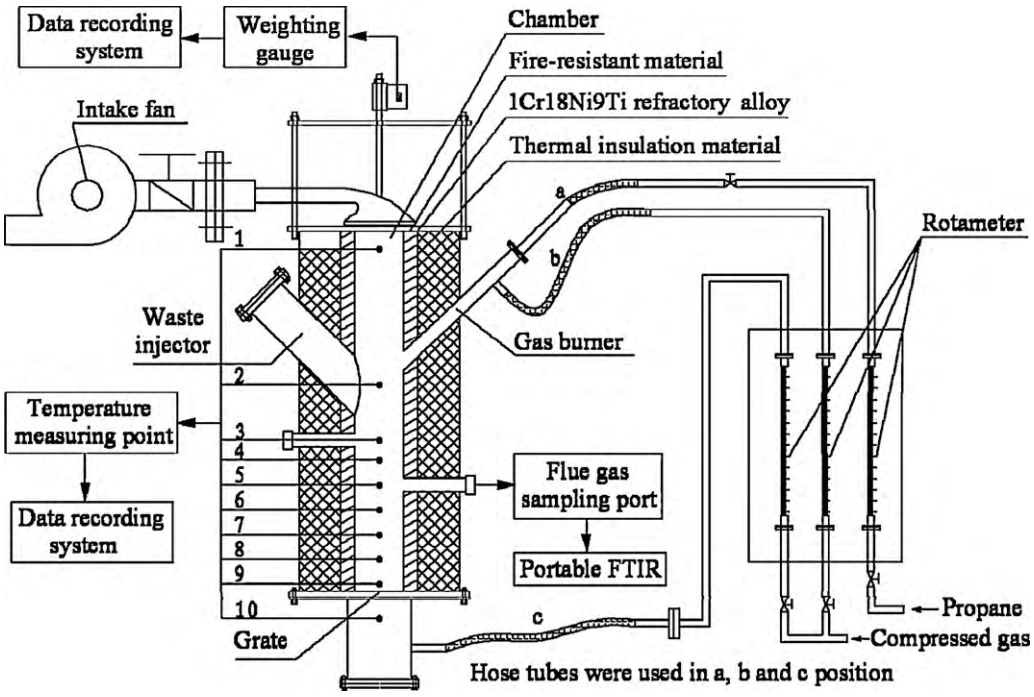

Fig. 3. Schematic diagram of the one-dimensional experimental facility.

nect a threaded sampling probe to sampling combustion gas, which is analyzed by a connecting portable FTIR. A gas burner at 750 mm above the grate is installed at 45° angle to the waste bed to ignite the waste and simulate radiation from the front arch and the combustion gas. The temperature of the chamber above the waste bed surface is supposed to be maintained at 900 °C during the experimental procedure. Primary air and air to the propane are supplied by a tank of compressed-air. Rotameters monitor flow rates of air and propane. To avoid errors during weight measuring, flexible gas tube junctions are used to the chamber. A draft fan withdraws flue gas in the chamber.

2.3. Instrumentation

Three systems of equipment record temperature, weight and gas composition measurements. The temperature measuring equipment includes ten thermocouples connected with a temperature monitoring system, which can link to a computer with RS-232 data access to record all temperatures during the experiment. The weight measuring equipment includes a weighing sensor and a weighing scale linked to a computer with RS-232 data access. The weighing scale has a resolution of 20 g. The gas composition equipment includes a sampling probe, a set of gas cleaning devices and a portable FTIR. The main parameters of the portable FTIR are as follows: wavelength range 900–4200 cm^{-1}, resolution 8 cm^{-1}, temperature of gas cell and pipe 180 °C, scanning frequency 10 times per second, volume of gas cell 1.07 L. The spectra of combustion gas are obtained while gas is pumped into the gas cell and then analyzed by software that comes with the portable FITR. We can obtain gas concentrations and digitally record spectra.

2.4. Specimen and experimental conditions

The Shanghai LüZou Environmental Protection Engineering Company provided specimens of hazardous wastes. The composition of each specimen were paint slag (24%), tar slag (27%), emulsion slag (29%), $Ca(OH)_2$ (13%) and paper (7%). Mixtures of these wastes were prepared by grinding into small pieces and extruded by a roller-forming machine. Properties of the waste mixtures and experimental conditions are shown separately in Tables 2 and 3. The primary air rate, the bed height and particle size varied, respectively, from 4 to 18 N m^3/h, from 300 to 600 mm and from 20 to 50 mm. Moisture content of the waste specimens was changed by placing specimens in a drying machine and evaporating some of the moisture at temperatures of 60, 70, 80 and 90 °C for about 8 h.

Before starting an experimental run, the weighing scale is set to zero and then specimens are pushed into the chamber from the waste injector. The waste injector is then locked to separate air

Table 1
Thermocouple positioning.

	No.									
	1	2	3	4	5	6	7	8	9	10
Height[a] (mm)	1238	748	548	478	388	298	208	118	28	−90

[a] Height means vertical distance of thermocouple above the grate.

Table 2
Composition and thermal characteristics of waste.

M_{ar} (%)	A_{ar} (%)	V_{daf} (%)	C_{ar} (%)	H_{ar} (%)	O_{ar} (%)	N_{ar} (%)	S_{ar} (%)	$Q_{net,ar}$ (kJ/kg)
33.49	23.77	81.14	28.83	3.17	10.63	0.07	0.04	10,145

Table 3
Experimental conditions.

No.	Primary air rate (N m³/h)	Moisture (%)	Ash (%)	Height (mm)	Particle size (mm)
1	4	19.98	28.60	500	50
2	6	19.34	28.83	500	50
3	10	20.15	28.54	500	50
4	14	20.80	28.31	500	50
5	18	20.70	27.63	500	50
6	14	25.93	26.48	500	50
7	14	15.93	30.05	500	50
8	14	12.57	31.25	500	50
9	14	20.87	28.28	300	50
10	14	20.87	28.28	400	50
11	14	21.63	28.01	600	50
12	14	21.73	27.26	500	20
13	14	21.47	27.35	500	30
14	14	20.22	28.51	500	40

and heat. When preparations are ready, propane is ignited and the chamber temperature rises rapidly to 900 °C. The propane flow is maintained at a steady value to keep the temperature fixed. The waste bed is immediately irradiated from the high temperature flame. Monitoring begins and all data are digitally recorded. After gas-phase burning was visually observed, primary air was allowed to flow into the chamber at a slowly increased rate until the desired value is reached.

To observe and investigate the different combustion characteristics of the specimen, thicker layer than normal grate furnace was adopted in the experiment, which extended the time period of the combustion. Hence, the whole experiment took longer time than that of normal grate furnace.

3. Results and discussion

3.1. The burning process

Case 4 is picked out, as shown in Table 3, to discuss the temperature distribution, the weight loss and the gas release during the combustion process. Temperatures over and within the bed are shown in Fig. 4. Temperatures of the propane flame (t2) rise quickly to 900 °C and are maintained at this temperature throughout the whole experimental process. Because of the radiation of propane flame, temperatures over the bed (t3) and on the bed surface (t4) start to rise immediately. From this moment on, the waste on the surface begins to evaporate and pyrolyze. The pyrolysis gas escapes from the bed and burns above it. Meanwhile, evaporation and pyrolysis start in the layer below. After ignition, these reactions migrate downward at a certain speed. After a period, temperatures in the middle of the bed (t5) start to rise, which can be measured by the first thermocouple in the bed layer. The rise in temperature indicates steady combustion in the bed. Then, in sequence, temperatures at t6–t9 start to rise until combustion is complete.

Two other observations should be noted. The first is that the maximum temperatures at t7 and t8 are much higher than those are at t5 and t6. This can be explained in the following manner. Under steady combustion, char produced from the previous stage and gas produced in the current stage would combust at the same time. However, there is not enough oxygen supply to complete combustion of both. As pyrolysis gas is in a lower layer than is char, oxygen supplies pyrolysis gas, and therefore completes combustion while char burns slowly and at a lower temperature because of the lack of oxygen. After a period, most of the pyrolysis gas in the bed is released and gets burnt, and a large quantity of char remains piled up in the bottom of the chamber. Without the combustion of pyrolysis gas, all available oxygen is consumed in the combustion of char, which greatly increases its burning rate. For this reason, temperatures at t7 and t8 rise so high. The second observation is that of the maximum temperatures recorded in the bed the lowest were recorded at t9. This is because of the cooling primary air flowing up through the grate. Fig. 4 also presents temperatures of flue gas. After the burning of propane, we can see that at t1 temperatures rise immediately over 400 °C with a subsequent increment to 500 °C after wastes have started burning.

Weight loss of case 4 from the bed is shown in Fig. 5 and indicates that the combustion process can be separated into three stages. The first stage corresponds to an ignition stage with minimal weight loss. The second stage manifests a steady weight loss rate. The third stage corresponds to completion of reactions, where weight loss rates fall to zero. The transitions between the three stages occur with a temperature increase at t5 and a decrease at t9.

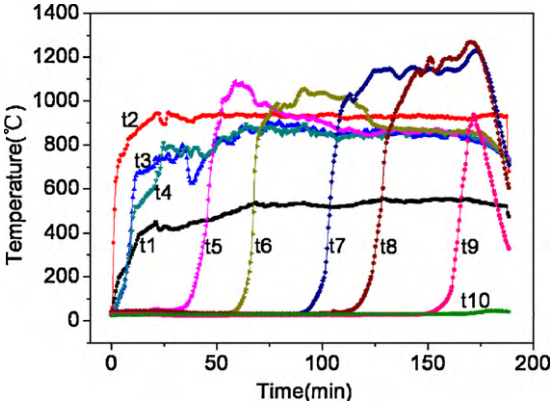

Fig. 4. Temperature distribution above and within the waste bed.

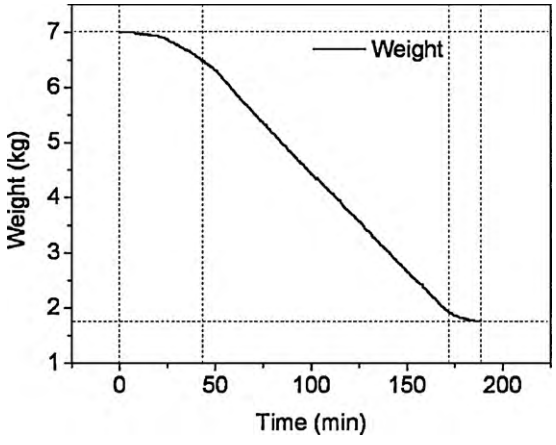

Fig. 5. Weight loss of the waste bed.

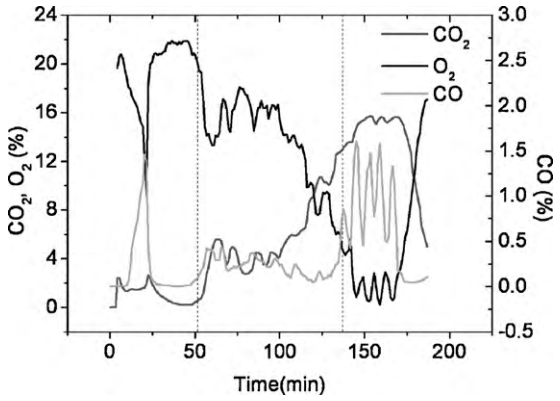

Fig. 6. Concentrations of CO_2, CO and O_2 during the experiment.

Concentrations of CO_2, CO and O_2 of case 4 are presented in Fig. 6. Gas distributions can also be divided into three stages, but in a different way to weight loss. The first stage occurs before ignition of the waste bed. In this stage, CO increases and then decreases rapidly. At the same time, O_2 concentrations have a very sharp fall and rise, while CO_2 concentrations have a small peak. These observations can be explained in the following manner. Before gas-phase combustion, pyrolysis gas releases from the bed and accumulates above the bed. At this moment, primary air has not been supplied. There is no gas flowing up but combustion propane and its air flowing down, which causes the pyrolysis gas to flow down into the bed. The gas sampling system pumps nothing out but pyrolysis gas as there is no other gases in the bed at this moment. However, moments later, pyrolysis gas starts to burn and supply of primary air commences. Gas drawn into the gas sampling system consists mostly of air from the bottom. Hence, we have a short period of little CO and CO_2, and more than 20% O_2, as can be observed in Fig. 6. The second stage in the evolution of the gas distribution is the period constituting mainly pyrolysis gas combustion in the bed marked by O_2 decreases and CO_2 increases. CO concentration levels are kept low. This occurs because char seldom burns in this stage and most of the O_2 fuels combustion of gas. The third stage is characterized mainly by char combustion with concentrations of O_2 being almost depleted and of CO suddenly rising. During this stage, most of the pyrolysis gas has burnt out. Much of the char left from the second stage starts to burn at a faster rate, thus needing much more O_2. Primary air is not in sufficient supply for combustion, so a large quantity of CO forms in the process. Towards the end, all combustible material burns out. CO_2 and CO levels decrease rapidly while O_2 increases rapidly.

Oscillations in gas concentrations were found in the whole measurement process. The reason is the following. The particle size in waste is roughly 50 mm, and there are a finite number of particles. Combustion of each particle is an independent process with different particle species being at different combustion stages.

3.2. Burning rate, weight loss percentage and ignition-front speed

3.2.1. Burning rate, weight loss percentage and ignition-front speed with different primary air rate

The burning rate mentioned in this work is the burning rate of the steady combustion occurring after ignition. Burning rates for different primary air rates are shown in Fig. 7(a). Blackened squares in the figure are experimental results and the red line is a parameter fit of experimental results. The burning rate initially increases, attains a maximum and then decreases with increasing primary air rate. At low primary air rates, combustion proceeds in a lean oxygen environment. The burning rate is essentially determined by the primary air rate, as observed in the figure. However, the burning rate cannot be ultimately sustained being limited by both the reaction rate and convective cooling by air. In consequence of pri-

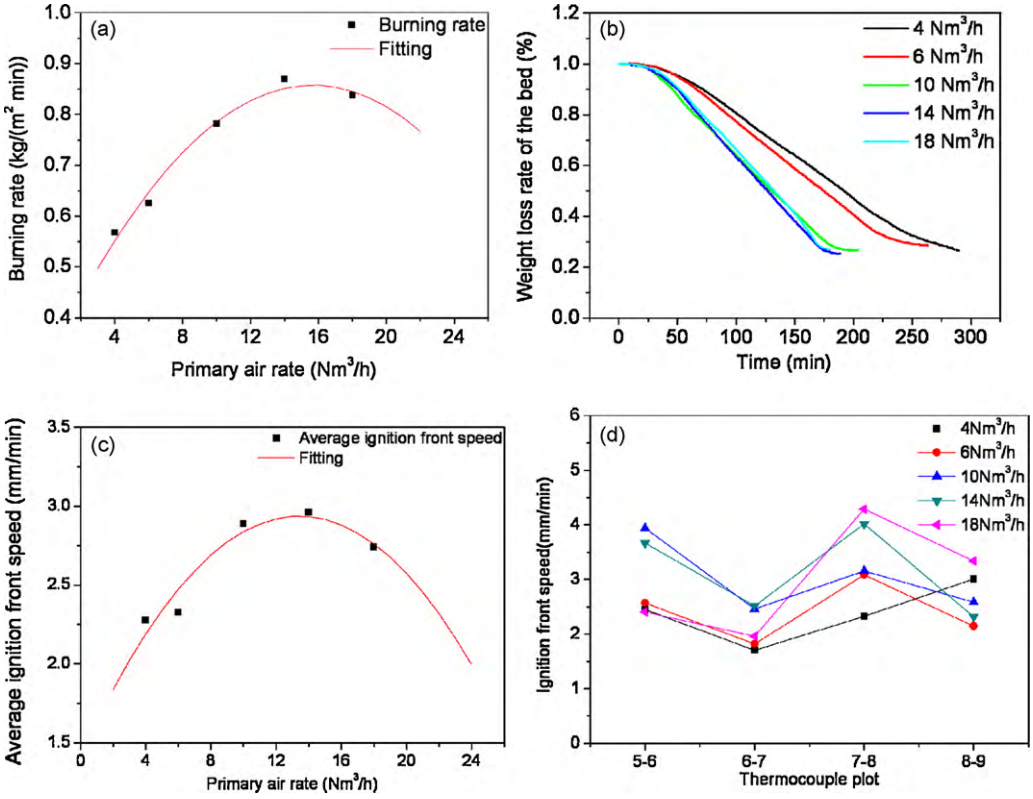

Fig. 7. Effect of primary air rate on burning rate, weight loss percentage and ignition-front speed.

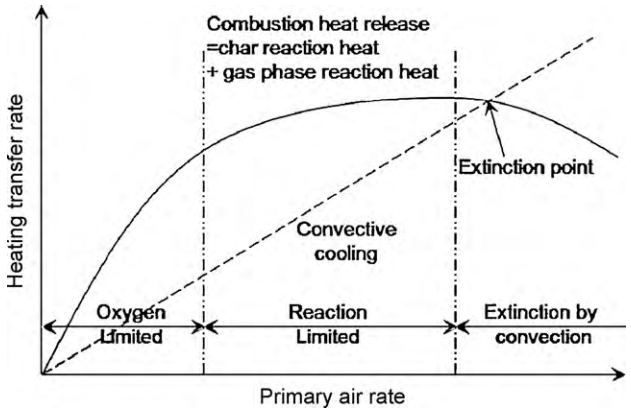

Fig. 8. Effect of primary air rate on the combustion of fixed bed.

mary air, reaction rate and convective cooling, a peak burning rate of 0.869 kg/(m^2 min) was observed at 14 N m^3/h. As the primary air rate keeps increasing, the effect of reaction rate and convective cooling assumes prominence over that of primary air rates. Therefore, burning rates start to decrease. The relationship of burning rates to these three impact factors can also be seen in Fig. 8. Again, we can divide the combustion process into three stages. The first is an oxygen-lean stage, in which the primary air rate is the more important factor that influences burning rates. With the increase in primary air rates, oxygen levels rise sufficiently to significantly affect reaction rates implicated in combustion. Peak burning rates appear within this stage while primary air rates keep increasing, enhancing convective cooling. At a particular moment, convective cooling balances combustion heat releases after which the bed fails to ignite [14–16].

The dependence of weight loss percentages on primary air rates is presented in Fig. 7(b). Weight loss rates are determined from gradients of the curves. Of note is that the weight loss rate for the 18 N m^2/h curve is initially smaller but finally larger than that for the 14 N m^2/h curve. This is because initially pyrolysis gas combustion predominates. Convective cooling for the 18 N m^3/h rate is too large at this stage. However, in the char combustion stage, more oxygen leads to faster combustion of char, and thereby a larger weight loss rate.

Average ignition-front speeds for different primary air rates are presented in Fig. 7(c). The overall trend is similar to that between burning rate and primary air rate. The average ignition-front speed reaches a peak average ignition-front speed at 14 N m^3/h. The reason is similar to that of burning rate for different primary air rate. The sectional ignition-front speeds are shown in Fig. 7(d). In the figure, a pair of numbers along the *x*-axis corresponds to consecutive thermocouple positions identifying a layer in the bed, while the *y*-axis represents average ignition-front speeds between these two positions. Combustion phases can also be divided by position. The 5-6 and 6-7 layers correspond to the pyrolysis gas combustion phase. The 7-8 layer correspond to the char combustion phase while the 8-9 layer correspond to the residue combustion phase. From the figure, a lot of information can be obtained. In the pyrolysis gas combustion phase, primary air rates that are two low or too high produce low ignition-front speeds while in the char combustion phase, higher primary air rates led to higher ignition-front speed. Ignition-front speeds in the residue combustion phase are more complicated. The ignition-front speed for a primary air rate of 18 N m^3/h in the 8-9 layer was high because of the intensive combustion in the 7-8 layer. The ignition-front speed for a 4 N m^3/h primary air rate is also high because oxygen can finally be supplied to the residue combustion, creating a less lean conditions in the excess air compared with fuel. Reaction rates are faster than previous. For the other three conditions, char has already been consumed and there is little remaining fuel, so ignition speeds are low.

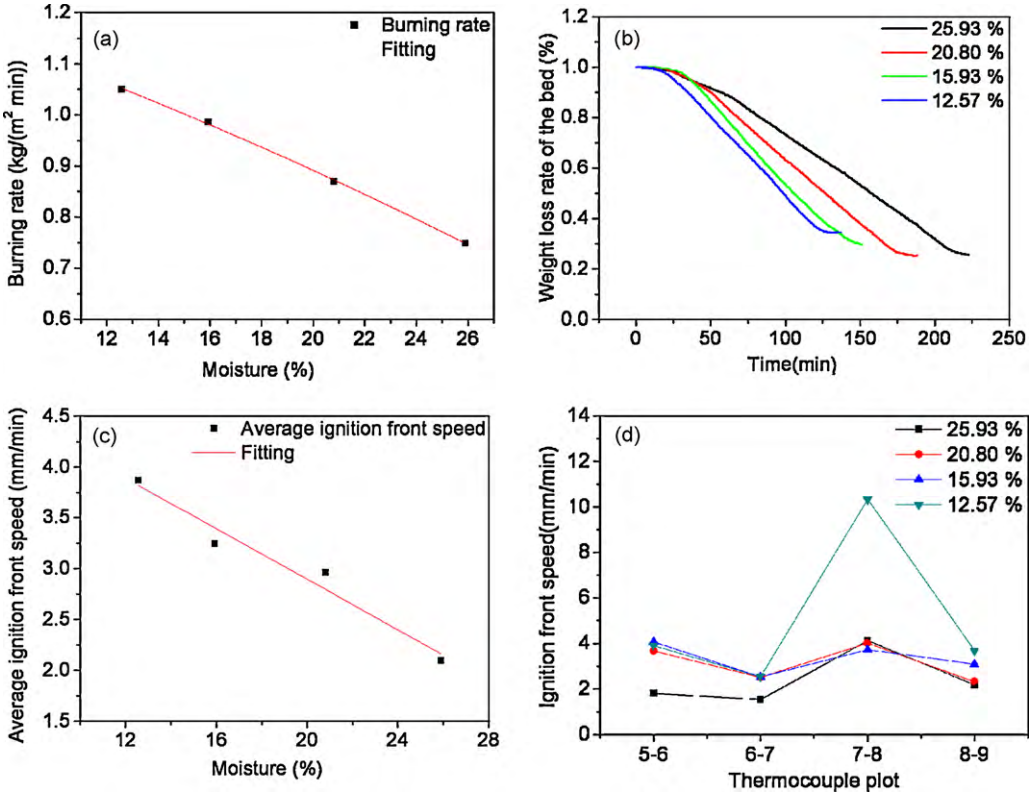

Fig. 9. Effect of moisture on burning rate, weight loss percentage and ignition-front speed.

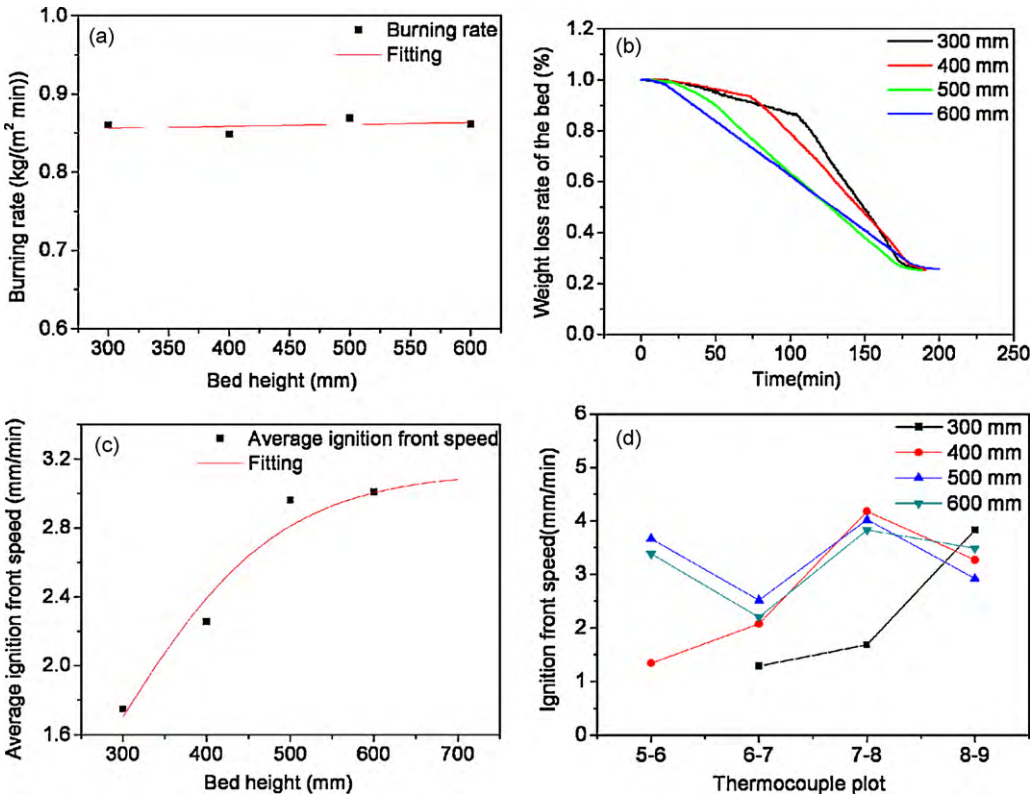

Fig. 10. Effect of bed height on burning rate, weight loss percentage and ignition-front speed.

3.2.2. Burning rate, weight loss percentage and ignition-front speed with different moisture

Results representing burning rates of waste with different percentage moisture content are presented in Fig. 9(a). The black squares represent experimental results and the red line is a fitted curve to the experimental data. Clearly, burning rates decrease almost linearly with increasing moisture content. This is because waste with higher moisture content needs additional energy to evaporate the moisture. The burning rate is thereby slowed down.

Weight loss percentages of the bed for different moisture content are presented in Fig. 9(b). Weight loss rate decreases with increasing moisture content, and has a similar trend and similar explanation as for variation in burning rates for different moisture content. We remark that every curve in the figure has a short stage with a different slope to the main weight loss stage. These correspond to conditions associated with the ignition stage and correlates longer ignition stage with higher moisture content. Again, more moisture in the waste leads to longer evaporation times.

The variation in average ignition-front speeds with moisture content is shown in Fig. 9(c). Obviously, an increase in moisture content decreases the average ignition-front speed because of longer evaporation times. The sectional ignition-front speeds are shown in Fig. 9(d). All ignition-front speeds are low for a moisture content of 25.9%, while those of 20.8% and 15.93% are similar in magnitude. Ignition-front speeds for moisture content of 12.57% take their highest values, particularly in the char combustion phase.

3.2.3. Burning rate, weight loss percentage and ignition-front speed with different bed heights

The variation of burning rates with bed height is shown in Fig. 10(a). Burning rates for the four bed heights are almost the same. This was to be expected as steady combustion at different bed heights was achieved under similar combustion conditions, i.e. same particle size, primary air rate and moisture, hence, yielding similar burning rates.

Weight loss percentages of the bed for different bed heights are shown in Fig. 10(b), from which weight loss rates are found to increase as bed height increases. Ignition stages appear with different gradients to the main weight loss stage that follows. These stages arise because of the changes in distance from the bed top surface to the propane flame. Different distances create different intensities in radiation from the propane flame, thus affecting ignition speeds. With the increase in bed height, distances diminish and radiation intensities become stronger, which promote faster ignition.

The variation in average ignition-front speeds with bed height is presented in Fig. 10(c). Average ignition-front speeds increased with increasing bed height. Shortening distances under different conditions lead to different radiation exposures from the propane flame, which causes these conditions to ignite at different rates. Shorter distances increased radiation intensities over the bed, making ignition easier. Sectional ignition-front speeds are shown in Fig. 10(d). Ignition-front speeds for both the 600 and 500 mm bed heights are similar. The ignition-front speed for the 400 mm bed height within the 5-6 layer is slower because the bed height is too low for rapid radiation-induced ignition. The slow ignition-front speed for a 300 mm bed height within the 6-7 layer results for a similar reason. However, at the other extreme, the ignition-front speed for this 300 mm height within the 8-9 layer is faster than other heights in the same layer but is slowest within the adjacent 7-8 layer. The explanation is that combustion is delayed because of poor irradiation over a lower bed surface. Hence, combustion is delayed in layers below and the char combustion and the pyrolysis gas combustion stages overlap. The ignition-front speed for the 300 mm bed height within the lower 8-9 layer actually indicates this intermingling.

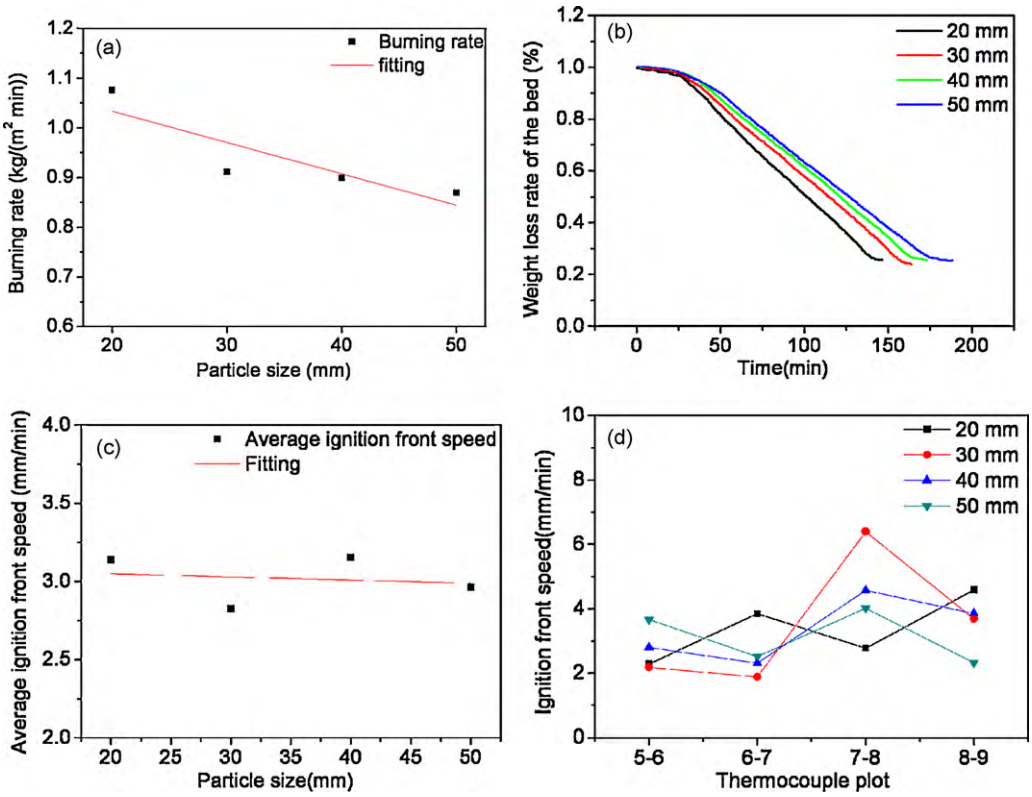

Fig. 11. Effect of particle size on burning rate, weight loss percentage and ignition-front speed.

3.2.4. Burning rate, weight loss percentage and ignition-front speed with different particle sizes

Burning rates for different particle sizes as shown in Fig. 11(a), are seen to decrease with increasing particle size. This can be understood as an increase in complexity and difficulty in heat transfer to the waste particle, making ignition of a single particle harder to achieve and waste bed combustion also to slow down. Weight loss percentages of the bed are shown in Fig. 11(b). With increasing particle size, the weight loss rate of the bed decreases, which also can be explained by burning rate trends.

The variation of average ignition-front speeds with particle size, shown in Fig. 11(c), shows that speeds remain roughly constant over all particle sizes. This indicates that particle size has little impact on average ignition-front speeds. However, findings are different for sectional ignition-front speeds. The ignition-front speed for 20 mm-sized particles was approximately twice as large as for other sizes in the 6-7 layer. Combustion is then occurring with particles of a smaller size and a much greater surface-to-volume ratio. Pyrolysis gas is released and gets burnt rapidly. Char on the surface of the particle burns in this stage, and as a result, there is an ash layer surrounding the char that delays the onset of char combustion reactions. Ignition-front speeds are then lower than for other conditions and furthermore lowers speeds in the char combustion stage. This process can also be alluded to in the highest temperatures measured at positions t6 and t8, as listed in Table 4. There, combustion can be observed from these two temperature readings. At position t6, it can be seen that the highest temperature of the 20 mm-sized particles is much higher than that for the other three, implying that combustion for the 20 mm-sized particles is much more intensive at the pyrolysis gas stage. At position t8, temperatures reverse with the 20 mm-sized particles having a temperature much lower than the other three, indicating that char combustion is weak. Trends observed in Fig. 11 are in accord with those extracted from Table 4. Trends in the other three particle sizes are discussed in the following. In the pyrolysis gas combustion stage, ignition-front speeds increase with increasing particle size with the exception of the 20 mm-sized particles. Despite the fact that larger particles have larger surface areas, more char actually covers particle surfaces thereby inhibiting combustion. The probability of reaction between char and oxygen is then lowered, leaving more oxygen to fuel the combustion of pyrolysis gas. This creates conditions whereby larger-sized particles are associated with higher ignition-front speeds. However, in the char combustion stage, trends are different. Char inside the particle surface burns in this stage. With lower available particle surface, abatement of reaction between oxygen and char occurs, and we can concur that ignition-front speeds are lower for larger-sized particles.

Table 4
Highest temperature readings for various particle sizes.

Highest temperature (°C)[a]	Particle size (mm)				Moisture (%)			
	20	30	40	50	12.57	15.93	20.80	25.93
Position								
6	1226	1110	1073	1052	965	1017	1052	1164
8	1204	1252	1265	1268	1354	1289	1268	1176

[a]Highest temperatures refer to readings taken at thermocouples t6 and t8.

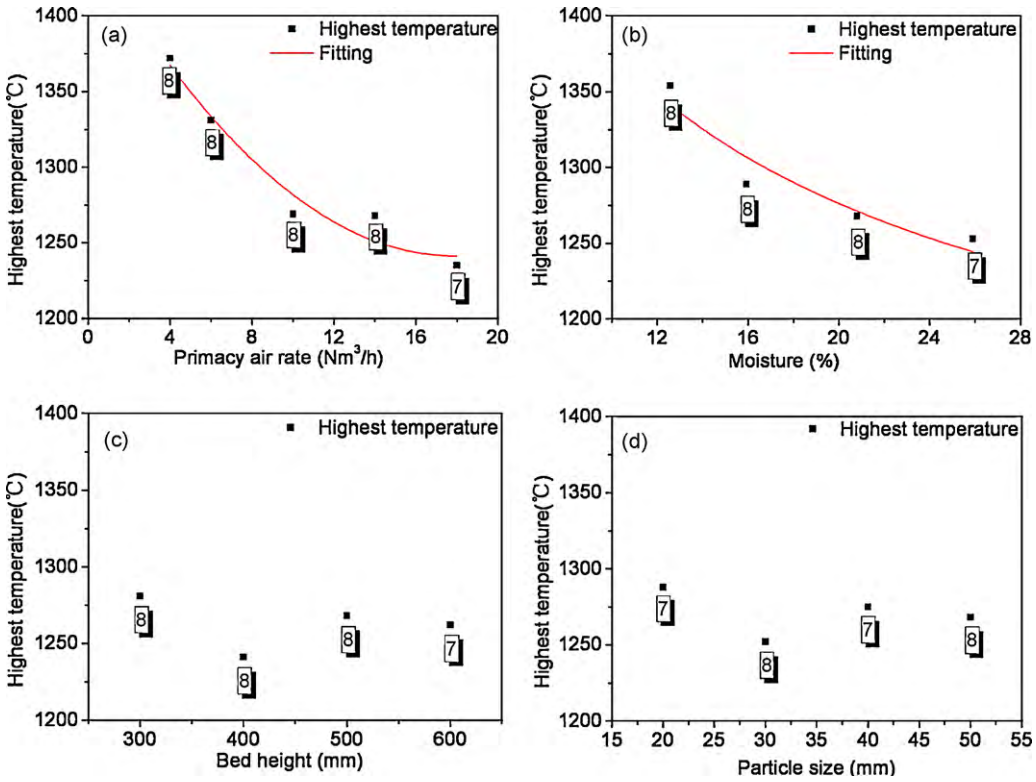

Fig. 12. Highest temperatures of the bed for conditions of different primary air rate, moisture, bed height and particle size.

3.3. The highest temperature and the corresponding position

Fig. 12(a)–(d) shows trends in highest temperatures in the bed layer with respect to primary air rate, moisture content, bed height and particle size, respectively. Black squares represent the highest temperature readings under the various conditions. The red-colored curves are the parameter fits to the experimental results. The numbers in the shadowed rectangles refer to the positions of the temperature readings. It can be seen from Fig. 12(a) that the highest temperature decreases with increasing primary air rate, indicating that char combustion conditions worsened because of the poor primary air rate. This causes more slagging, as well as deterioration in the heat transfer and thus raising temperatures. Another observation to be remarked upon is that the highest temperature for the rate 18 N m^3/h occurs only for position t7. The reason is that a large volume of primary air cools the thermocouple at position t8, thereby lowering its temperature below that of position t7.

Fig. 12(b) indicates that with increasing moisture content, highest temperatures decrease. As found earlier, higher moisture content slows the burning rate, and energy produced from combustion is transferred immediately, thus lowering temperatures in the bed. The highest temperature for 25.9% moisture was found at position t7, while for other values this occurs at position t8 due to the lower burning rates. In this environment, some char can ignite in the pyrolysis gas combustion stage. The temperature of position t6 is higher than the other three conditions, as can be seen in Table 4. In addition, cooling from primary air affects the combustion for the 25.9% moisture content more than for the drier conditions. Temperatures at position t8 are cooled, hence, for 25.9% moisture, the highest temperature occur at position t7.

Variation of highest temperatures with bed height is shown in Fig. 12(c). From the figure, changes in highest temperatures are not as noticeable compared with other factors and no correlation of highest temperature with position, and therefore bed height, is observed.

Fig. 12(d) presents the variation of highest temperature with particle size. No obvious trend is seen and therefore no relationship between highest temperature and particle size results. However, all highest temperatures were found at position t8 except for 20 mm-sized particles. This can also be explained by arguments mentioned in Section 3.2.4. The pyrolysis gas combustion stage for 20 mm-sized particles is more intensive and highest temperatures must then appear earlier.

4. Conclusion

The combustion characteristics of particles of hazardous waste mixtures in a fixed bed were investigated to simulate the combustion characteristics of waste in grate furnaces. A rising temperature front descended through the bed. Combustion was divided into three stages according to weight loss rates.

Burning rates and average ignition-front speeds first increased and then decreased with increasing primary air rate. Weight loss rates increased with increasing primary air rate except at 18 N m^3/h. In the pyrolysis gas combustion phase, primary air rate that were too low or too high caused lower ignition-front speeds. In the char combustion phase, a higher primary air rate led to higher ignition-front speeds.

Burning rate, weight loss rate and average ignition-front speed decreased with the increase in moisture. All ignition-front speeds corresponding to moisture content of 25.9% were low, while those of 20.8% and 15.93% were similar. Ignition-front speeds were highest for the lower moisture content of 12.57%.

Burning rates were essentially independent of bed height. Weight loss rate and average ignition-front speed increased with increasing bed height. All ignition-front speeds for both 600 and

500 mm bed heights were similar. Ignition-front speeds were lower for the 400 mm bed height within the 5-6 layer and for the 300 mm bed height within the 6-7 layer. The ignition-front speed for 300 mm bed height within the 8-9 layer was higher than other speeds within the same 8-9 layer but lower than other speeds within the 7-8 layer.

Burning rates and weight loss rates decreased with increasing particle size. The average ignition-front speeds for different particle sizes were similar. The ignition-front speed corresponding to 20 mm-sized particles show a different behavior to the other three. In the pyrolysis gas combustion stage, the ignition-front speed increased with increasing particle size except for 20 mm particle sizes. However, in the char combustion stage, larger particle sizes produced slower ignition-front speeds.

Highest temperatures decreased with increasing primary air rates and moisture content. Changes in highest temperatures were essentially independent of bed heights and particle sizes. No trends in highest temperatures were discernible.

References

[1] C.J. Yang, C.Q. Hu, Studies of tar slag utilization, Fuel Chem. Process. 35 (2004) 39–40 (in Chinese).
[2] T.H. Liou, Pyrolysis kinetics of electronic packaging material in a nitrogen atmosphere, J. Hazard. Mater. 103 (2003) 107–123.
[3] R. Bassilakis, R.M. Carangelo, M.A. Wójtowicz, TG–FTIR analysis of biomass pyrolysis, Fuel 80 (2001) 1765–1786.
[4] J.H. Yan, H.M. Zhu, X.G. Jiang, Y. Chi, K.F. Cen, Analysis of volatile species kinetics during typical medical materials pyrolysis using a distributed activation energy model, J. Hazard. Mater. 162 (2009) 646–651.
[5] H.M. Zhu, J.H. Yan, X.G. Jiang, Y.E. Lai, K.F. Cen, Study on pyrolysis of typical medical waste materials by using TG–FTIR analysis, J. Hazard. Mater. 153 (2008) 670–676.
[6] Z.Q. Liu, J.H. Li, Y.F. Nie, Development trend and policy analysis on prevention and control technology of hazardous waste pollution in China, China Environ. Protect. Ind. 6 (2000) 12–14 (in Chinese).
[7] Y.B. Yang, H. Yamauchi, V. Nasserzadeh, J. Swithenbank, Effects of fuel devolatilisation on the combustion of wood chips and incineration of simulated municipal solid wastes in a packed bed, Fuel 82 (2003) 2205–2221.
[8] D. Shin, S. Choi, The combustion of simulated waste particles in a fixed bed, Combust. Flame 121 (2000) 167–180.
[9] C. Ryu, Y.B. Yang, A. Khor, N.E. Yates, V.N. Sharifi, J. Swithenbank, Effect of fuel properties on biomass combustion: Part I. Experiments—fuel type, equivalence ratio and particle size, Fuel 85 (2006) 1039–1046.
[10] Y.B Yang, V.N. Sharifi, J. Swithenbank, Effect of air flow rate and fuel moisture on the burning behaviours of biomass and simulated municipal solid wastes in packed beds, Fuel 83 (2004) 1553–1562.
[11] H. Zhou, A.D. Jensen, P. Glarborg, P.A. Jensen, A. Kavaliauskas, Numerical modeling of straw combustion in a fixed bed, Fuel 84 (2005) 389–403.
[12] Z.Q. Li, C.L. Liu, Z.C. Chen, J. Qian, W. Zhao, Q.Y. Zhu, Analysis of coals and biomass pyrolysis using the distributed activation energy model, Bioresource Technol. 100 (2009) 948–952.
[13] Z.Q. Li., Corn Straw and Biomass Blends: Combustion Characteristics and NO Formation. Nova Science Publishers, Inc., New York, USA, 2009.
[14] H. Thunman, B. Leckner, Influence of size and density of fuel on combustion in a packed bed, Proc. Combust. Inst. 30 (2005) 2939–2946.
[15] H. Frey, B. Peters, H. Hunsinger, J. Vehlow, Characterization of municipal solid waste combustion in a grate furnace, Waste Manag. 23 (2003) 689–701.
[16] Y.B. Yang, C. Ryu, A. Khor, V.N. Sharifi, J. Swithenbank, Fuel size effect on pinewood combustion in a packed bed, Fuel 84 (2005) 2026–2038.